Development of Magnetorheological Dampers with Embedded Piezoelectric Force Sensors for Structural Vibration Control

S. W. Or,[1] Y. F. Duan,[2] Y. Q. Ni,[2,*] Z. H. Chen[2] and K. H. Lam[1,2]

[1]*Department of Applied Physics, The Hong Kong Polytechnic University Hung Hom, Kowloon, Hong Kong*

[2]*Department of Civil and Structural Engineering, The Hong Kong Polytechnic University Hung Hom, Kowloon, Hong Kong*

ABSTRACT: Magnetorheological (MR) dampers with embedded piezoelectric force sensors are developed to enable real-time, closed-loop vibration control of civil and mechanical structures. In this study, a prestress-type piezoelectric force sensor is fabricated and integrated with an actuation-only MR damper to form a smart MR damper possessing the attractive functionality of force sensing-while-damping with a high degree of sensor–damper collocation. Calibration of the piezoelectric force sensor is performed in a servohydraulic material testing system operating in force-controlled excitations of sine and ramp waveforms at different combinations of amplitude and frequency. The sensing and damping performance of the smart MR damper is evaluated by operating the material testing system in displacement-controlled sine and ramp excitations while adjusting different DC control currents to the damper. A good agreement between the piezoelectric force sensor outputs and the material testing system force inputs is observed, besides the highly controllable force–displacement and force–velocity hysteretic characteristics. The results show great promise of deploying the smart MR damper in intelligent structural vibration control systems.

Key Words: intelligent systems, magnetorheological (MR) damper, piezoelectric force sensor, sensor–damper collocation, smart MR damper, structural vibration control.

INTRODUCTION

Magnetorheological (MR) dampers have been used in vibration control of civil and mechanical structures. Application examples include vibration control of the stay cables in cable-stayed bridges (Ni et al., 2002a,b,c; Johnson et al., 2003; Ko et al., 2003, 2005; Duan, 2004; Duan et al., 2005a,b, 2006), seismic protection of buildings and other full-scale structures (Dyke et al., 1996, 1998; Spencer et al., 1997a; Yang, 2001; Hiemenz et al., 2003), vibration damping of automotive seats and suspension systems (Choi et al., 2000; Han et al., 2002), and vibration isolation of automated machines (Carlson, 2000), to name a few.

As shown in Figure 1, a state-of-the-art MR damper (Dyke et al., 1998; Snyder et al., 2001) generally consists of a cylindrical housing with MR fluid, a bearing and seal unit, an electromagnet, a pair of electrical wires extended from the electromagnet, a diaphragm, an accumulator, a piston, an upper connection support, and a lower connection support. The bearing and seal unit guides the movement of the piston (and the upper connection support) with respect to the cylindrical housing (and the lower connection support) and prevents the leakage of the MR fluid. The accumulator compensates the change of volume due to the movement of the piston, thereby avoiding the presence of cavities within the MR fluid. The diaphragm, which acts as the moving part of the accumulator, separates the MR fluid from the accumulator. The MR fluid has the ability to reversibly change its rheological characteristics upon applying a magnetic field. In more detail, the MR fluid is capable of changing itself from a free-flowing, linear-viscous state to a semi-solid state with controllable yield stress in milliseconds when exposed to an applied magnetic field (Carlson and Weiss, 1994). By inputting different electrical control currents to the electromagnet through the electrical wires of such an MR damper, the magnetic fields applied to the enclosed MR fluid can be changed accordingly so that the yield stress associated with the MR fluid and hence the damping force of the MR damper can be readily controlled in milliseconds.

While possessing controllable damping force capability, the existing MR dampers (Figure 1) are incapable of self-sensing of structural vibrations or external forces; they are used in an open-loop mode of operation instead (Duan, 2004; Duan et al., 2005a, 2006), and their

*Author to whom correspondence should be addressed.
E-mail: ceyqni@polyu.edu.hk
Figures 4, 10 and 13 appear in color online: http://jim.sagepub.com

1045-389X/08/11 1327–12 $10.00/0 DOI: 10.1177/1045389X07085673

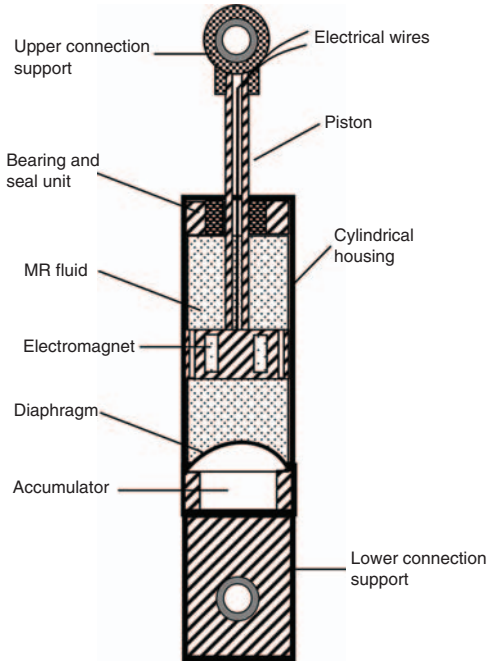

Figure 1. *Schematic diagram of conventional MR damper.*

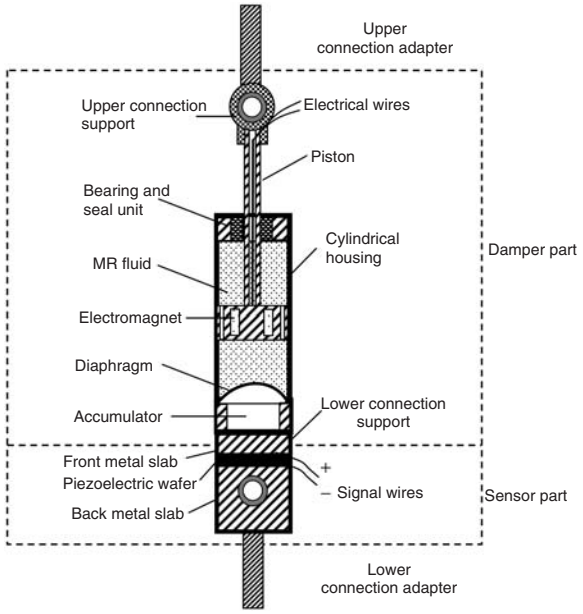

Figure 2. *Schematic diagram of prestress-type piezoelectric force sensor-based smart MR damper.*

controllable capability cannot be fully utilized. In fact, the advance of structural vibration control technology from an open-loop operation to a closed-loop operation of MR dampers may be made by developing an accurate inverse dynamic model for the dampers so as to determine an appropriate control current for the facilitation of the corresponding damping force (Chang and Zhou, 2002; Tsang et al., 2006). Nevertheless, it is still a challenge to develop such an inverse dynamic model for the highly nonlinear dampers (Spencer et al., 1997b; Jin et al., 2005). Alternatively, a force feedback control loop (Dyke et al., 1996; Christenson, 2001) is often deployed to overcome the deficiency of inverse dynamic modeling via the installation of individual force sensors between the vibrating structures and the MR dampers at the expense of reducing the control effectiveness and increasing both the implementation difficulty and engineering cost. Therefore, it is highly desirable to develop smart MR dampers with embedded force sensors for providing real-time, force-feedback control in a relatively simple, cost-effective, and reliable manner.

Piezoelectric materials can convert changes in mechanical energy into electrical signal and can also exhibit the converse effect. The direct piezoelectric effect has enabled the extensive use of the materials in commercial force sensors with sufficiently high sensitivity, large dynamic range, good reliability, and lightweight (Or et al., 1998, 2005; Chiu et al., 2003). By designing a specific piezoelectric force sensor, and with an appropriate integration with an actuation-only MR damper, it is technologically viable to develop a smart MR damper for real-time monitoring of forces acting on the damper through the measurement of the generated piezoelectric signal. Moreover, this piezoelectrically induced signal can be utilized to adjust the corresponding electrical current (or the magnetic field) applied to the damper (or the enclosed MR fluid) and thereby control the damping force for the vibrating structure. In this study, the authors describe the structure and operating principle of a prestress-type piezoelectric force sensor-based smart MR damper and report the fabrication, calibration, sensing, and damping performance of such a prototype smart MR damper.

STRUCTURE AND OPERATING PRINCIPLE

Figure 2 shows the schematic diagram of the prestress-type piezoelectric force sensor-based smart MR damper. This is composed of a damper part, a sensor part, and a connection adapter part. The damper part originates from an actuation-only MR damper. It basically follows the structure and operating principle of the conventional MR damper shown in Figure 1 and comprises a cylindrical housing with MR fluid, a bearing and seal unit, an electromagnet, a pair of electrical wires extended from the electromagnet, a diaphragm, an accumulator, a piston, an upper connection support, and a lower connection support. The sensor part is essentially a prestress-type piezoelectric force sensor attached axially to the lower connection support of the damper part. The adoption of the prestress design allows a better

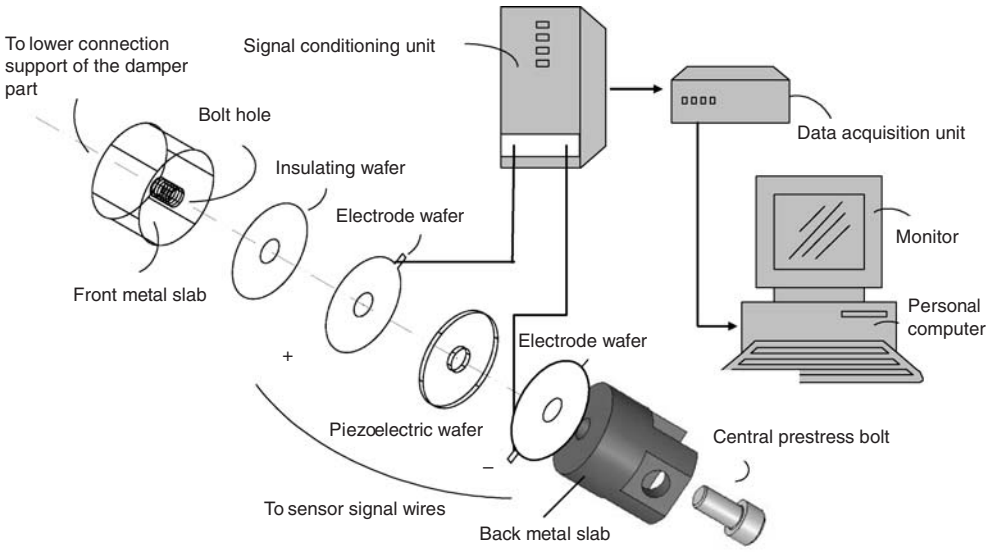

Figure 3. *Details of prestress-type piezoelectric force sensor.*

accommodation of elevated dynamic stresses without causing fracture failure of the sensor structure. Figure 3 illustrates the details of the prestress-type piezoelectric force sensor outlined in Figure 2. It is seen that there are two electrode wafers positioned on the two sides of the piezoelectric wafer to provide external connections with the sensor signal wires. The electrode wafer on the left-hand side is set as the positive electrode while the one on the right-hand side is taken to be the negative or ground electrode. As these sensor components are to be sandwiched by a front metal slab and a back metal slab, the insertion of an insulating wafer between the front metal slab and the positive electrode is required to prevent short-circuiting of the piezoelectric wafer and the whole sensor. Since there exist very high interfacial stresses between the component interfaces, and by considering that the strength of materials is usually much greater in compression than in tension, the sandwich is liable to fracture failure during the expansion phases of oscillations (especially when subjected to elevated tensile forces). By mechanically biasing the sensor with a central prestress bolt, the tensile strength of the whole sensor is increased and the possibility of fracture failure can be reduced. Referring to Figure 2, the connection adapter part, which has an upper connection adapter and a lower connection adapter connecting the upper connection support of the damper part and the back metal slab of the sensor part, respectively, permits the installation of the whole smart MR damper to the desired vibrating structure or test equipment.

In operation, the sensor part senses the variation in external force exerted on the smart MR damper due to structural vibration and produces piezoelectric signal (i.e., piezoelectric charge) with amplitude proportional to, and frequency the same as, the variance in external force. This piezoelectrically induced signal can be processed and used to assist in controlling the electrical current to the damper part so that the controlled damping force can be provided to the vibrating structure in a real-time, closed-loop means. This enables the structural vibration force to be monitored in the operation of the smart MR damper.

FABRICATION

The piezoelectric material selected for the piezoelectric wafer is a moderately hard lead zirconate titanate (PZT) piezoceramic (Ferroperm Pz28). Table 1 shows some important material parameters of Ferroperm Pz28. This material possesses the distinct advantages of high electromechanical coupling ($k_{33} = 0.687$), strong piezoelectric activity ($g_{33} = 31.4\,\text{mV.m/N}$), low dielectric loss ($\tan\,\delta_e = 0.4\%$), high stress handling capability ($Y_{33}^E = 54.7\,\text{GPa}$), and high thermal stability ($T_c > 330^\circ\text{C}$). The piezoelectric wafer has an outer diameter of 38 mm, an inner diameter of 13 mm, and a thickness of 2 mm. It is coated with silver electrodes on the two main surfaces perpendicular to its thickness, and electric polarization is induced along the thickness direction using these electrode surfaces. The insulating wafer, in the form of a ring with a larger outer diameter of 40 mm, a smaller inner diameter of 10 mm, and a much smaller thickness of 0.1 mm, is made of polyimide. The electrode wafers, also in ring shape, are prepared from a beryllium–copper (Be–Cu) alloy sheet to have the same outer and inner diameters as the insulating wafer but with a half-reduced thickness of 0.05 mm. The front and back metal slabs, which are made of stainless steel 304, have a diameter of 42 mm and a length of 45 mm. The central prestress bolt is a standard M10 high-tension bolt.

Table 1. Some important material parameters of Ferroperm Pz28 piezoceramic.

Material property	Value
Electromechanical coupling coefficient, k_{33}	0.687
Piezoelectric coefficient, g_{33} (mV·m/N)	31.4
Dielectric loss, tan δ_e (%)	0.4
Young's modulus, Y_{33}^E (GPa)	54.7
Curie temperature, T_c (°C)	>330

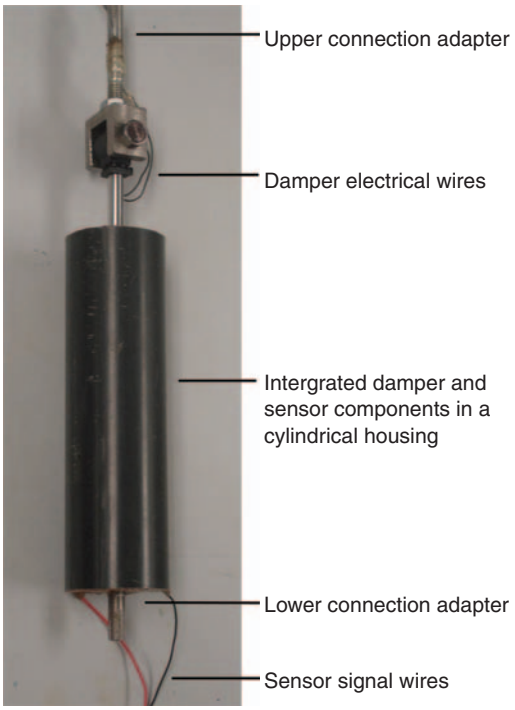

Figure 4. *Prototype of devised smart MR damper.*

By arranging the sensor components prepared above in accordance with Figure 3, the prestress-type piezoelectric force sensor (i.e., the sensor part) as shown in Figure 2 is assembled by applying an axial compressive prestress of 20 MPa to the piezoelectric force sensor assembly. This is done by exerting a calibrated torque of ≈40 Nm to the central prestress bolt using a torque driver (BRITOOL). It is noted that the applied prestress level of 20 MPa is specifically determined and optimized in such a way that it is high enough to provide the ultimate tensile force of ≈20 kN without leading to fracture failure of the sensor structure (i.e., 5 kN for the maximum operating tensile force of the damper part) and is low enough to avoid depolarization and breakage of the piezoelectric wafer. The assembled sensor is evaluated (to be reported in the next section) and then integrated with both the damper part and the connection adapter part according to the arrangement of Figure 2. Figure 4 shows the prototype of the smart MR damper schematized in Figures 2 and 3, whereas Table 2 summarizes the main specifications of the smart MR damper. It is noted that

Table 2. Main specifications of smart MR damper.

Diameter of housing (mm)	50
Length of housing (mm)	250
Maximum stroke (mm)	±12
Gap size (mm)	0.1
Turns of coil	5000
Maximum input current (A)	1.5

the major components of the damper and sensor parts are further enclosed by a cylindrical housing with a diameter of 50 mm and a length of 250 mm. The maximum stroke, gap size, turns of coil, and maximum input current are designated to be ±12 mm, 0.1 mm, 5000, and 1.5 A, respectively.

FORCE SENSOR PERFORMANCE

Capacitance Spectrum

The capacitance spectrum of the assembled piezoelectric force sensor is measured using a broadband dielectric spectrometer (Novocontrol Concept80). Figure 5 plots the frequency dependence of the capacitance. It is clear that the capacitance of the sensor has quite small variations from 4.5 to 5.4 nF with no prominent resonances in the desired operating frequency range of 0.1–30 Hz. This suggests that the sensor has sufficiently flat frequency response and broad operating frequency range for the detection of dynamic forces in various types of large civil and mechanical structures.

Charge-to-Force Sensitivity

The piezoelectric force sensor is calibrated by evaluating its charge-to-force ($Q-F$) sensitivity with a servohydraulic material testing system (MTS 810) operating in force-controlled excitations of sine and ramp waveforms at 16 different combinations of force amplitudes (i.e., 500, 1000, 1500, and 2000 N) and frequencies (i.e., 0.2, 1, 5, and 10 Hz). The experimental setup is shown in Figure 6. The piezoelectric force sensor is mounted onto the material testing system using the upper and lower grippers. The piezoelectric charges developed by the sensor due to the excitation forces of the material testing system are measured using a charge meter (Kistler 5015A). All signals are sampled and recorded by a computer-controlled data acquisition system (National Instruments 635E).

Figure 7 shows the time domain waveforms and $X-Y$ plots of the material testing system's force input and the piezoelectric force sensor's charge output under different force-controlled sine excitations of 500, 1000, 1500, and 2000 N amplitudes and at 1 Hz frequency. Figure 8 reports the results of the cases when the sensor is subject

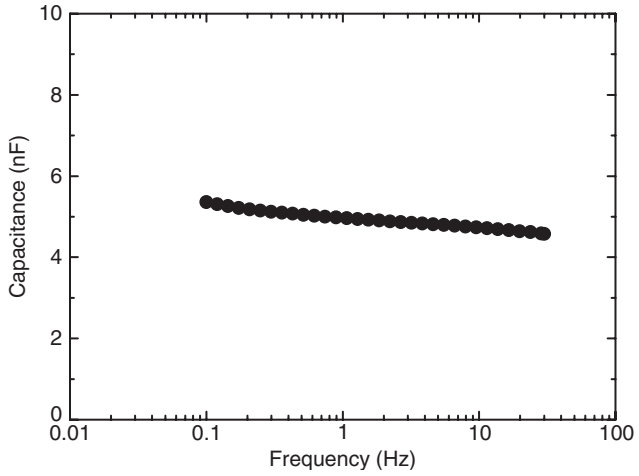

Figure 5. *Capacitance spectrum of piezoelectric force sensor in smart MR damper.*

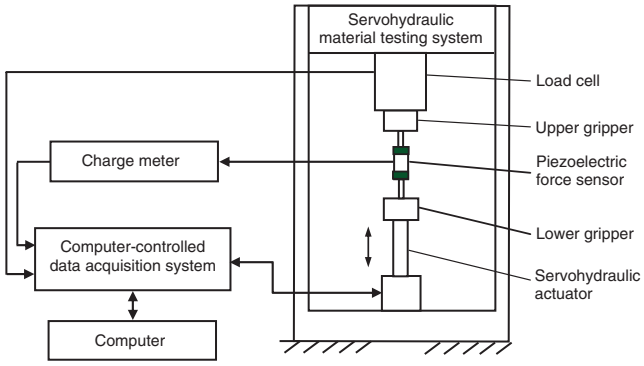

Figure 6. *Experimental setup for calibration of charge-to-force sensitivity of piezoelectric force sensor.*

to the force-controlled ramp excitations. It should be mentioned that the compressive forces are defined as positive so that the force and charge waveforms as shown in Figures 7 and 8 are of the same phase for ease of comparison. From the time domain waveforms (Figures 7 and 8), it is obvious that the piezoelectric force sensor's charge outputs agree well with the material testing system's force inputs in terms of amplitude and phase. This agreement is further supported by their $X-Y$ plots (Figures 7 and 8) where the charge–force relationships are essentially linear with minimal hysteretic effect. Based on the linear relationships of charge and force (i.e., the $X-Y$ plots), the sensitivity of the piezoelectric force sensor, characterized by the charge-to-force coefficient (k), can be determined by minimizing the summation of square residual (Π) as follows:

$$\Pi = \sum_{i=1}^{n} (Q_i - kF_i)^2 \tag{1}$$

where i indicates the sampling sequence and n is the total number of data used for the $X-Y$ plot. To quantify the magnitude of the residual, the relative residual ($\delta_{(Q,kF)}$) is defined as:

$$\delta_{(Q,kF)} = \sqrt{\frac{1}{n}\sum_{i=1}^{n}(Q_i - kF_i)^2} \Big/ \sqrt{\frac{1}{n}\sum_{i=1}^{n} Q_i^2} \tag{2}$$

Tables 3 and 4 summarize the values of k and $\delta_{(Q,kF)}$ resulting from the 16 different combinations of force amplitudes (i.e., 500, 1000, 1500, and 2000 N) and frequencies (i.e., 0.2, 1, 5, and 10 Hz) under the force-controlled sine and ramp excitations, respectively. It is found that the variation in k is reasonably small, as evidenced by a few percent of $\delta_{(Q,kF)}$. Figure 9 shows the frequency dependence of k based on the data presented in Tables 3 and 4. As there is no manifest dispersion effect on k, the mean value of k ($\bar{k}$) is found to be 142.9 pC/N with a small standard deviation of 0.0129. In practice, the structural vibration force exerted on the piezoelectric force sensor can be determined as long as the piezoelectric charge is measured and the following correlation holds true:

$$F = \frac{Q}{\bar{k}}. \tag{3}$$

SMART MR DAMPER PERFORMANCE

Force Sensing

The force sensing performance of the smart MR damper is evaluated by operating the same material testing system in displacement-controlled sine and ramp excitations of 5 mm displacement amplitude, 5 Hz frequency, and with different DC control currents of 0, 0.5, 1, and 1.5 A applied to the damper. Figure 10 illustrates the schematic diagram and photograph of the experimental setup. Figures 11 and 12 show the comparison between the forces obtained by the piezoelectric force sensor and the material testing system under displacement-controlled sine and ramp excitations, respectively. For each type of excitation (Table 5), there exists a good agreement with only a few percent of relative difference between the two forces ($\delta_{(F,Q/\bar{k})}$) (except for the case with null control current), according to the following expression:

$$\delta_{(F,Q/\bar{k})} = \sqrt{\frac{1}{n}\sum_{i=1}^{n}(F_i - Q_i/\bar{k})^2} \Big/ \sqrt{\frac{1}{n}\sum_{i=1}^{n} F_i^2} \tag{4}$$

where i indicates the sampling sequence and n is the total number of data used for the calculation. The reason for the relatively big difference in the absence of the DC

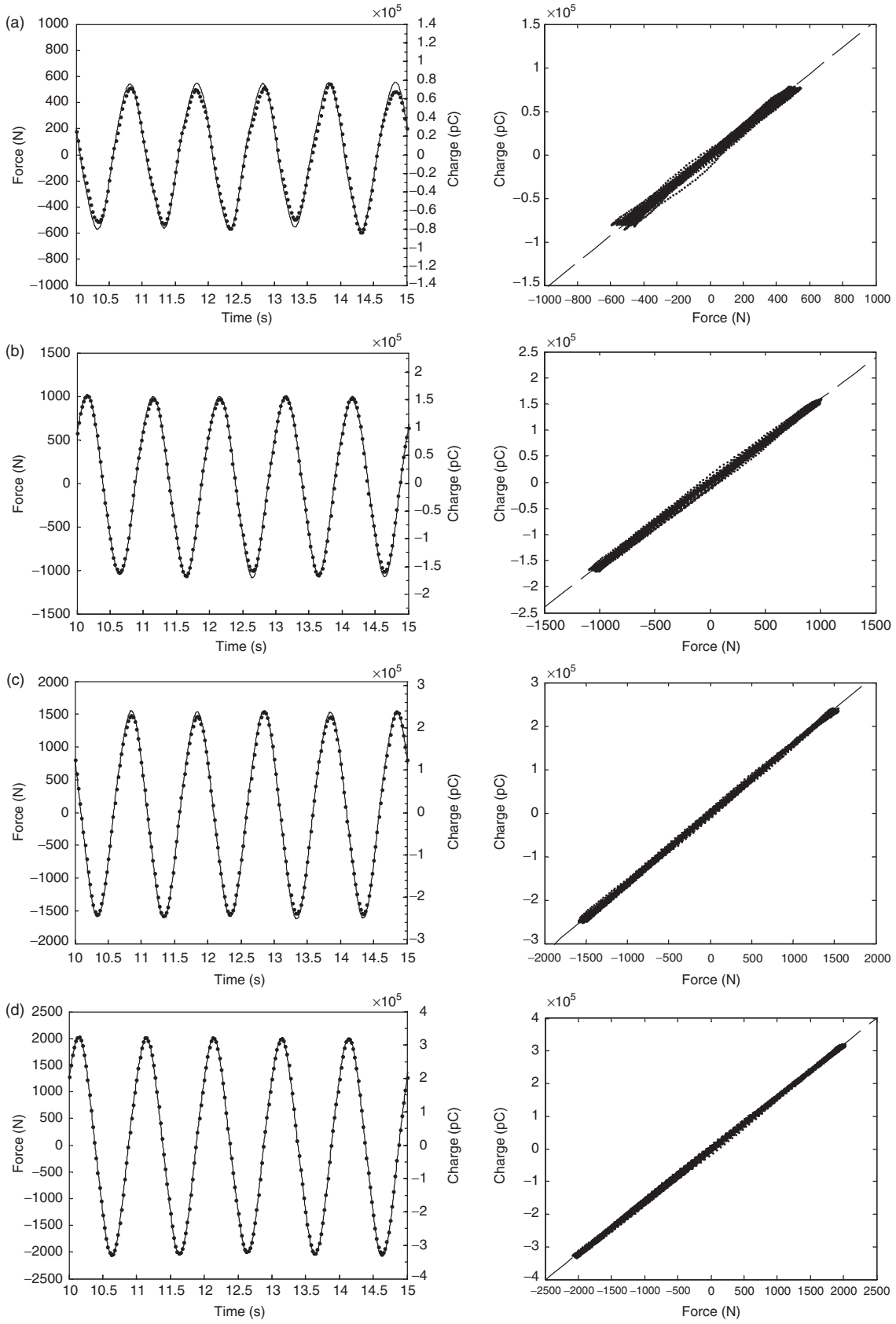

Figure 7. *Calibration of piezoelectric force sensor under various force-controlled excitations of sine waveform at 1 Hz frequency and (a) 500 N, (b) 1000 N, (c) 1500 N, and (d) 2000 N amplitudes. The dot '.' and line '—' associated with the time domain waveforms on the left-hand side represent the material testing system's force input and the piezoelectric force sensor's charge output, respectively. The dot '.' and dashed line '- -' associated with the X – Y plots on the right-hand side are the experimental data and the linearly fitted lines, respectively.*

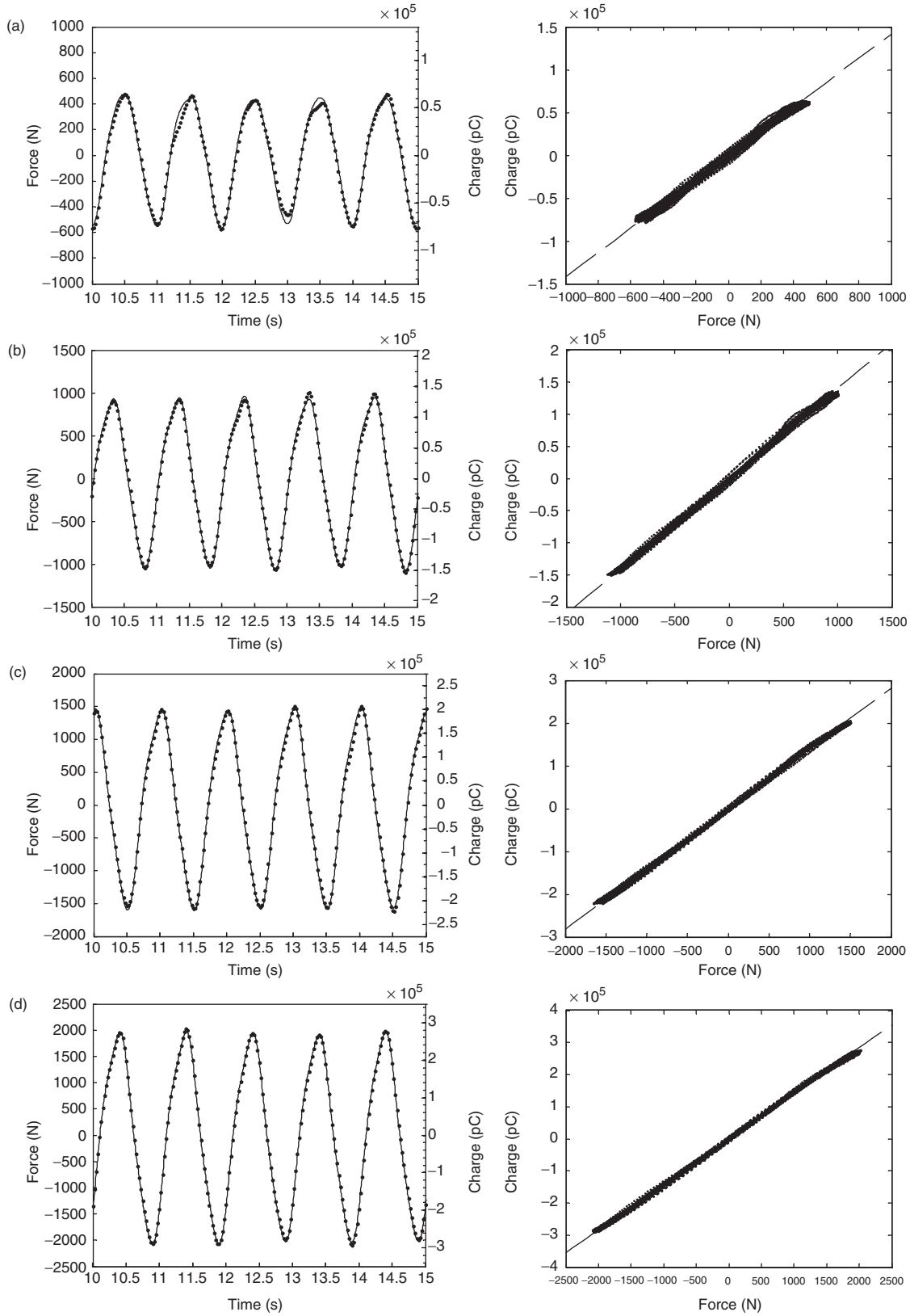

Figure 8. *Calibration of piezoelectric force sensor under various force-controlled excitations of ramp waveform at 1 Hz frequency and (a) 500 N, (b) 1000 N, (c) 1500 N, and (d) 2000 N amplitudes. The dot '.' and line '—' associated with the time domain waveforms on the left-hand side represent the material testing system's force input and the piezoelectric force sensor's charge output, respectively. The dot '.' and dashed line '- -' associated with the X – Y plots on the right-hand side are the experimental data and the linearly fitted lines, respectively.*

Table 3. k and $\delta_{(Q,kF)}$ resulting from different combinations of force amplitude and frequency under force-controlled sine excitations.

Force (N)	Frequency (Hz) 0.2		1		5		10	
	k (pC/N)	$\delta_{(Q,kF)}$	*k* (pC/N)	$\delta_{(Q,kF)}$	*k* (pC/N)	$\delta_{(Q,kF)}$	*k* (pC/N)	$\delta_{(Q,kF)}$
500	134.51	0.0459	146.71	0.1012	148.50	0.1085	144.12	0.0609
1000	135.99	0.0338	151.12	0.0439	147.96	0.0517	143.90	0.0570
1500	136.35	0.0170	151.51	0.0263	148.54	0.0396	148.02	0.0752
2000	137.07	0.0133	151.89	0.0253	148.94	0.0286	146.98	0.0723

Table 4. k and $\delta_{(Q,kF)}$ resulting from different combinations of force amplitude and frequency under force-controlled ramp excitations.

Force (N)	Frequency (Hz) 0.2		1		5		10	
	k (pC/N)	$\delta_{(Q,kF)}$	*k* (pC/N)	$\delta_{(Q,kF)}$	*k* (pC/N)	$\delta_{(Q,kF)}$	*k* (pC/N)	$\delta_{(Q,kF)}$
500	136.06	0.0724	134.27	0.0850	146.85	0.1454	143.17	0.0580
1000	136.29	0.0432	133.25	0.0461	146.78	0.0651	143.40	0.0566
1500	136.63	0.0415	133.32	0.0333	147.95	0.0474	145.69	0.1002
2000	136.79	0.0292	134.68	0.0293	148.28	0.0356	146.49	0.0752

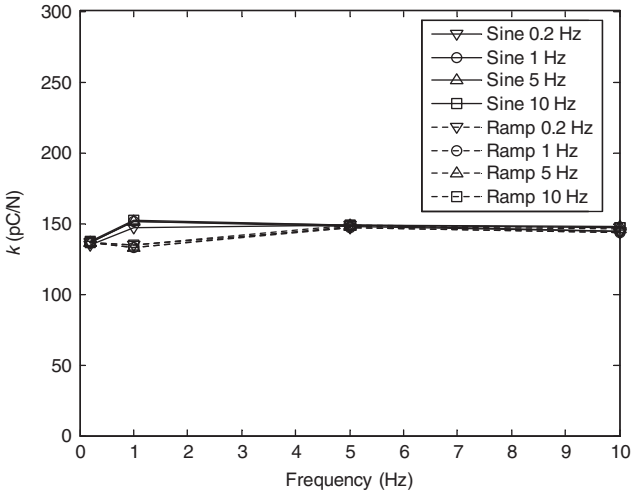

Figure 9. *Charge-to-force coefficient (k) as a function of frequency for various force-controlled excitations of sine and ramp waveforms at different combinations of amplitude (500, 1000, 1500, and 2000 N) and frequency (0.2, 1, 5, and 10 Hz).*

control current may be attributed to the courser resolution (i.e., 10 N) of the force sensor pre-installed in the material testing system compared to the actual damper force to be measured. Thus, the piezoelectric force sensor embedded in the smart MR damper provides better measurements.

Controllable Damping Force

Figure 13 shows the force–displacement and force–velocity hysteretic characteristics of the smart MR

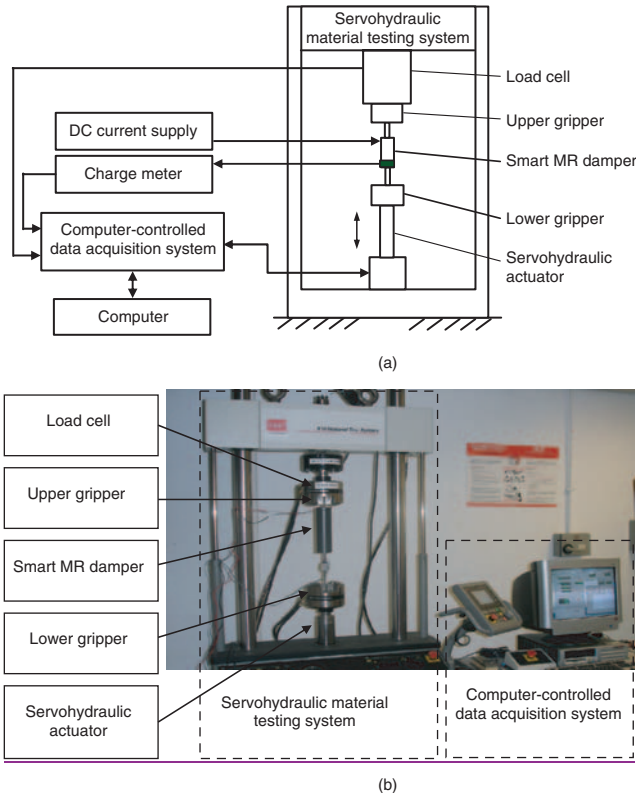

Figure 10. *Experimental setup for evaluation of sensing and damping performance of smart MR damper: (a) schematic diagram and (b) photograph.*

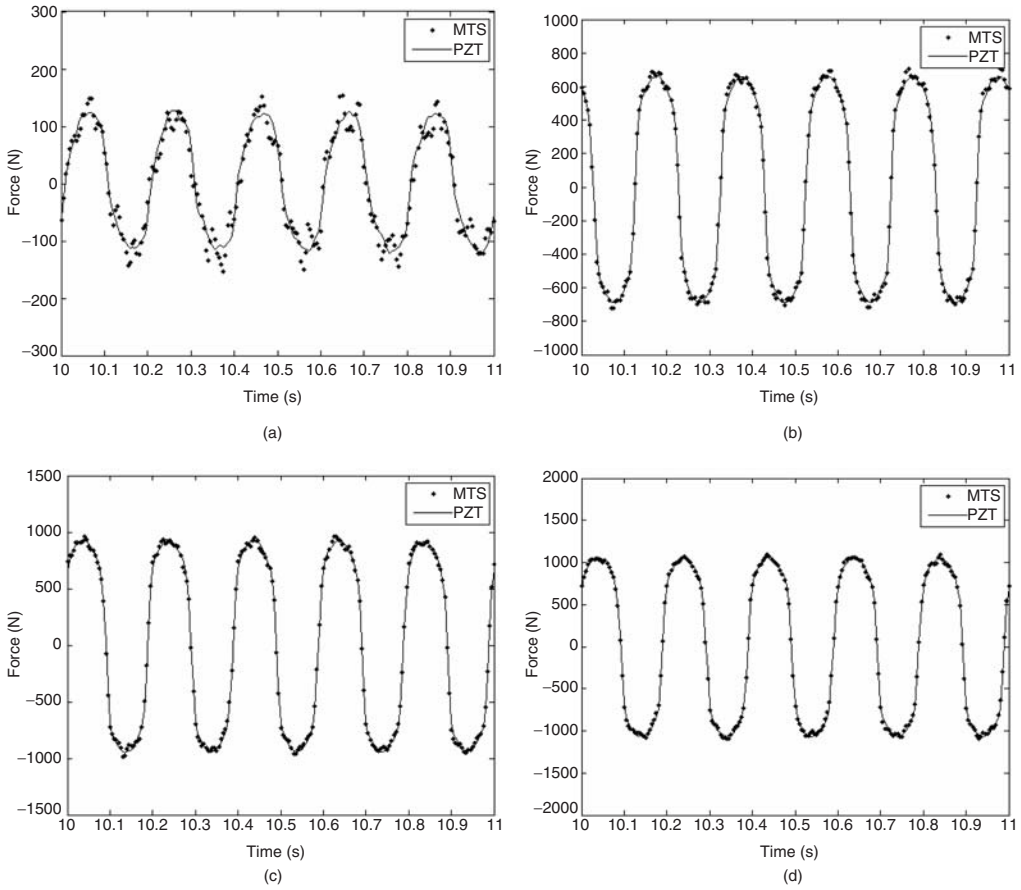

Figure 11. *Comparison between the forces obtained by piezoelectric force sensor and material testing system under displacement-controlled excitations of sine waveform at 5 mm amplitude, 5 Hz frequency, and with different DC control currents of (a) 0, (b) 0.5, (c) 1, and (d) 1.5 A applied to the damper.*

damper under displacement-controlled sine excitations of 5 mm amplitude, 5 Hz frequency, and with different DC control currents of 0, 0.5, 1, and 1.5 A applied to the damper. It is seen that the damping force increases appreciably from 75 to 600 N when the DC control current is increased from 0 to 0.5 A. The increasing trend tends to slow down when the DC control current is set beyond 0.5 A, and becomes almost unchanged at elevated DC control currents of >1 A owing to the effect of magnetic saturation. The observations suggest that the damping force depends on the control current applied to the damper. That is, the higher the control current applied, the larger the damping force obtained. Consequently, the tests indicate controllable damping forces of up to ≈1000 N under vibration amplitude of 5 mm and vibration frequency of 5 Hz. Such performance fulfils the usual application requirements for large civil and mechanical structures. For example, in the suppression of wind-rain-induced cable vibrations in a cable-stayed bridge (Duan et al., 2007), the upper limit of vibration frequency is no more than several hertz (even for short cables of <100 m long) and the vibration amplitude at the attachment location of the dampers is no more than several millimeters.

CONCLUSIONS

A smart MR damper possessing an attractive functionality of force sensing-while-damping with a high degree of sensor–damper collocation has been successfully developed by integrating a prestress-type piezoelectric force sensor with an actuation-only MR damper. The embedded piezoelectric force sensor has shown a flat frequency response over a broad operating frequency range of 0.1–30 Hz, together with a high charge-to-force coefficient of ≈143 pC/N under various force-controlled excitations of sine and ramp waveforms at 0.2–10 Hz frequencies and 500–2000 N amplitudes. The smart MR damper has demonstrated excellent force sensing and controllable damping force performance when subjected to displacement-controlled sine and ramp excitations and with different DC control currents. Importantly, this smart MR damper can directly relieve the technical challenge to develop complicated inverse

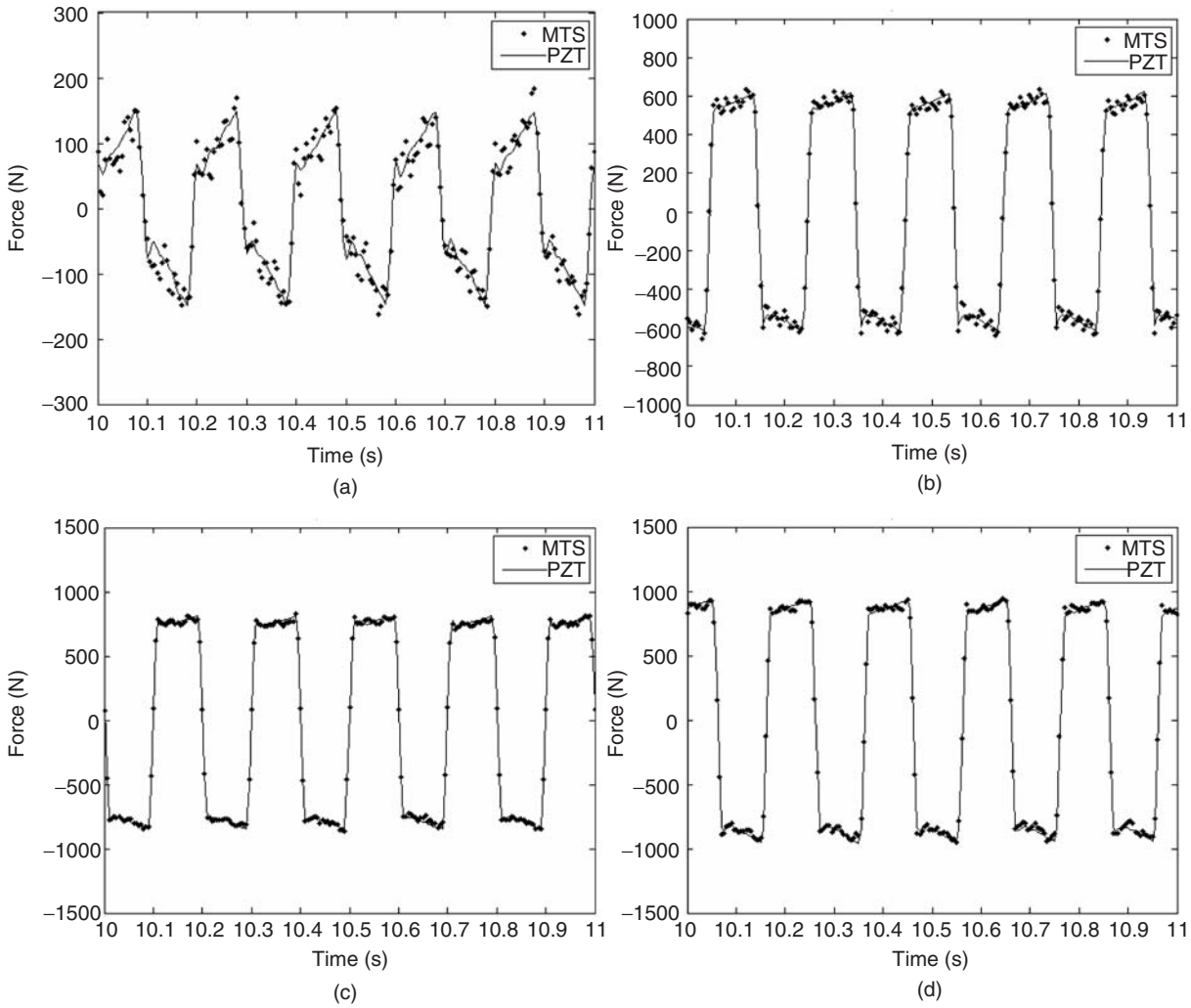

Figure 12. *Comparison between the forces obtained by piezoelectric force sensor and material testing system under displacement-controlled excitations of ramp waveform at 5 mm amplitude, 5 Hz frequency, and with different DC control currents of (a) 0, (b) 0.5, (c) 1, and (d) 1.5 A applied to the damper.*

Table 5. Relative differences between the forces obtained by piezoelectric force sensor and material testing system under displacement-controlled excitations.

DC control current (A)		0	0.5	1	1.5
$\delta_{(F,Q/\bar{k})}$	Sine excitation	0.2488	0.0467	0.0418	0.0402
	Ramp excitation	0.2170	0.0666	0.0339	0.0566

dynamic models for highly nonlinear actuation-only MR dampers on the one hand; it can provide a relatively simple, cost-effective, and reliable solution to the related communities on the other. Research efforts are in progress with the main aim of applying this smart MR damper to real-time, closed-loop vibration control of large civil and mechanical structures, particularly in vibration control of the stay cables in cable-stayed bridges and vibration damping of driver and passenger seats in automotive vehicles. Technical emphasis is being put on the optimization of the damper's architecture and performance against the integrity, durability, and cost-effectiveness associated with manufacturing and implementation. For instance, the integrity and durability of both the sensor and the damper parts are being improved using advanced manufacturing and integration techniques; the sensing performance is being refined via an optimization between structure, dimensions, and materials; the damping performance is being modified to better fit with the application requirements. Development of miniature and embeddable integrated-circuit (IC)-based controllers for further integration with the smart MR damper is an emphasis towards the next generation of intelligent MR damper.

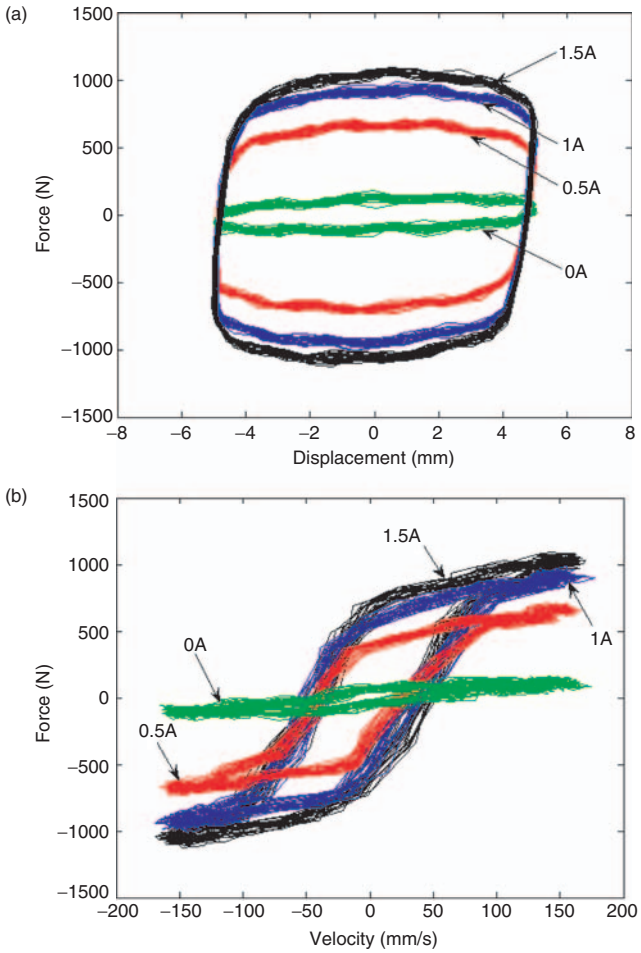

Figure 13. *Hysteretic characteristics of the smart MR damper under displacement-controlled sine excitations of 5 mm amplitude, 5 Hz frequency, and with different DC control currents of 0, 0.5, 1, and 1.5 A applied to the damper: (a) force versus displacement and (b) force versus velocity.*

ACKNOWLEDGMENTS

This work was supported by The Hong Kong Polytechnic University under Central Research Grant No. G-YD85 and Niche Areas Project No. I-BB95.

REFERENCES

Carlson, J.D. and Weiss, K.D. 1994. "A Growing Attraction to Magnetic Fluids," *Machine Design*, 66(August):61–66.

Carlson, J.D. 2000. "Washing Machine Having a Controllable Field Responsive Damper," US Patent, 6,151,930.

Chang, C.C. and Zhou, L. 2002. "Neural Network Emulation of Inverse Dynamics for a Magnetorheological Damper," *Journal of Structural Engineering*, ASCE, 128:231–239.

Chiu, S.S., Chan, H.L.W., Or, S.W., Cheung, Y.M. and Liu, P.C.K. 2003. "Effect of Electrode Pattern on the Outputs of Piezosensors for Wire Bonding Process Control," *Materials Science and Engineering B: Solid State Materials for Advanced Technology*, 99:121–126.

Choi, S.B., Nam, M.H. and Lee, B.K. 2000. "Vibration Control of a MR Seat Damper for Commercial Vehicles," *Journal of Intelligent Material Systems and Structures*, 11:936–944.

Christenson, R.E. 2001. "Semiactive Control of Civil Structures for Natural Hazard Mitigation: Analytical and Experimental Studies," PhD Dissertation, Department of Civil Engineering and Geological Sciences, University of Notre Dame, Notre Dame, Indiana, USA.

Duan, Y.F. 2004. "Vibration Control of Stay Cables Using Semi-Active Magneto-Rheological (MR) Dampers," PhD Dissertation, Department of Civil and Structural Engineering, The Hong Kong Polytechnic University, Hong Kong.

Duan, Y.F., Ni, Y.Q. and Ko, J.M. 2005a. "Design Guidelines for Open-Loop Vibration Control of Stay Cables Using MR Dampers," In: Tomizuka, M. (ed.), *Smart Structures and Materials 2005: Sensors and Smart Structures Technologies for Civil, Mechanical, and Aerospace Systems*, SPIE, Bellingham, Vol. 5765, pp. 678–689.

Duan, Y.F., Ni, Y.Q. and Ko, J.M. 2005b. "State-Derivative Feedback Control of Cable Vibration Using Semiactive Magnetorheological Dampers," *Computer-Aided Civil and Infrastructure Engineering*, 20:431–449.

Duan, Y.F., Ni, Y.Q. and Ko, J.M. 2006. "Cable Vibration Control Using Magnetorheological Dampers," *Journal of Intelligent Material Systems and Structures*, 17:321–325.

Duan, Y.F., Ni, Y.Q. and Ko, J.M. 2007. "Preliminary Design of Magneto-Rheological (MR) Dampers for Vibration Control of Stay Cables on Cable-Stayed Sutong Bridge," *Proceedings of the 4th Cross-strait Conference on Conference on Structural and Geotechnical Engineering*, Hangzhou, China, pp. 844–856.

Dyke, S.J., Spencer Jr, B.F., Sain, M.K. and Carlson, J.D. 1996. "Modeling and Control of Magnetorheological Dampers for Seismic Response Reduction," *Smart Materials and Structures*, 5:565–575.

Dyke, S.J., Spencer Jr, B.F., Sain, M.K. and Carlson, J.D. 1998. "An Experimental Study of MR Dampers for Seismic Protection," *Smart Materials and Structures*, 7:693–703.

Han, Y.M., Nam, M.H., Han, S.S., Lee, H.G. and Choi, S.B. 2002. "Vibration Control Evaluation of a Commercial Vehicle Featuring MR Seat Damper," *Journal of Intelligent Material Systems and Structures*, 13:575–579.

Hiemenz, G.J., Choi, Y.T. and Wereley, N.M. 2003. "Seismic Control of Civil Structures Utilizing Semi-Active MR Braces," *Computer-Aided Civil and Infrastructure Engineering*, 18:31–44.

Jin, G., Sain, M.K. and Spencer, B.F. 2005. "Nonlinear Blackbox Modeling of MR-Dampers for Civil Structural Control," *IEEE Transactions on Control Systems Technology*, 13:345–355.

Johnson, E.A., Christenson, R.E. and Spencer Jr., B.F. 2003. "Semiactive Damping of Cables with Sag," *Computer-Aided Civil and Infrastructure Engineering*, 18:132–146.

Ko, J.M., Ni, Y.Q., Chen, Z.Q. and Spencer Jr, B.F. 2003. "Implementation of MR Dampers to Dongting Lake Bridge for Cable Vibration Mitigation," In: Casciati, F. (ed.), *Proceedings of the 3rd World Conference on Structural Control*, John Wiley & Sons, Chichester, Vol. 3, pp. 777–786.

Ko, J.M., Duan, Y.F. and Ni, Y.Q. 2005. "Modeling of a Full-Scale MR Damper and Its Application in Open-Loop Vibration Control of Stay Cables," In: Tomizuka, M. (ed.), *Smart Structures and Materials 2005: Sensors and Smart Structures Technologies for Civil, Mechanical, and Aerospace Systems*, SPIE, Bellingham, Vol. 5765, pp. 690–700.

Ni, Y.Q., Chen, Y., Ko, J.M. and Cao, D.Q. 2002a. "Neuro-Control of Cable Vibration Using Semi-Active Magneto-Rheological Dampers," *Engineering Structures*, 24:295–307.

Ni, Y.Q., Duan, Y.F., Chen, Z.Q. and Ko, J.M. 2002b. "Damping Identification of MR-damped Bridge Cables from *In-Situ* Monitoring under Wind-Rain-Excited Conditions," In: Liu, S.-C.

(ed.), *Smart Structures and Materials 2002: Smart Systems for Bridges, Structures, and Highways*, SPIE, Bellingham, Vol. 4696, pp. 41–51.

Ni, Y.Q., Ko, J.M., Chen, Z.Q. and Spencer Jr., B.F. 2002c. "Lessons Learned from Application of Semi-Active MR Dampers to Bridge Cables for Wind-Rain-Induced Vibration Control," In: *Proceedings of China-Japan Workshop on Vibration Control and Health Monitoring of Structures*, Shanghai, China (in CD format).

Or, S.W., Chan, H.L.W., Lo, V.C. and Yuen, C.W. 1998. "Ultrasonic Wire-Bond Quality Monitoring Using Piezoelectric Sensor," *Sensors and Actuators A: Physical*, 65:69–75.

Or, S.W., Chan, H.L.W. and Liu, P.C.K. 2005. "Development of Smart Transducer with Embedded Sensor for Automatic Process Control of Ultrasonic Wire Bonding," *Smart Structures and Systems*, 1:47–61.

Snyder, R.A., Kamath, G.M. and Wereley, N.M. 2001. "Characterization and Analysis of Magnetorheological Damper Behavior under Sinusoidal Loading," *AIAA Journal*, 39:1240–1253.

Spencer Jr, B.F., Carlson, J.D., Sain, M.K. and Yang, G. 1997a. "On the Current Status of Magnetorheological Dampers: Seismic Protection of Full-Scale Structures," In: *Proceedings of American Control Conference*, New Mexico, USA, pp. 458–462.

Spencer, B.F., Dyke, S.J., Sain, M.K. and Carlson, J.D. 1997b. "Phenomenological Model for Magnetorheological Dampers," *Journal of Engineering Mechanics*, ASCE, 123:230–238.

Tsang, H.H., Su, R.K.L. and Chandler, A.M. 2006. "Simplified Inverse Dynamics Models for MR Fluid Dampers," *Engineering Structures*, 28:327–341.

Yang, G. 2001. "Large-Scale Magnetorheological Fluid Damper for Vibration Mitigation: Modeling, Testing and Control," PhD Dissertation, Department of Civil Engineering and Geological Sciences, University of Notre Dame, Notre Dame, Indiana, USA.